CHEMSUSCHEM

DOI: 10.1002/cssc.201100716

# A Method for Screening the Potential of MOFs as $CO_2$ Adsorbents in Pressure Swing Adsorption Processes

Gerhard D. Pirngruber,*[a] Lomig Hamon,[a] Sandrine Bourrelly,[b] Philip L. Llewellyn,[b] Estelle Lenoir,[b] Vincent Guillerm,[c] Christian Serre,[c] and Thomas Devic[c]

This work reports the adsorption and coadsorption data of $CO_2$/$CH_4$/CO mixtures on several metal–organic frameworks [MOFs; MIL-100(Cr), MIL-47(V), MIL-140(Zr)-A, Cu-btc, and MIL-53(Cr)] and compares them with reference adsorbents, that is, zeolite NaX and an activated carbon material, AC35. We also evaluate the effect of $H_2O$ on $CO_2$ adsorption and on the stability of the structures. Based on the experimental adsorption data, the performance potential of MOFs in several pressure swing adsorption processes is estimated by making a ranking of working capacities and separation factors. We discuss the separation of biogas, the purification of $H_2$ produced by steam reforming of methane, and the removal of $CO_2$ from synthesis gas in IGCC (integrated gasification combined cycle) systems. Some MOFs are very well placed in the ranking of (isothermal) working capacity vs. selectivity. Yet, performance is not the only criterion for the selection of MOFs. Ease and cost of synthesis and long-term stability are other important aspects that have to be taken into account.

## Introduction

$CO_2$ separation processes have been used in the chemical industry for a very long time. Two prominent examples are the removal of $CO_2$ from natural gas and from synthesis gas. Depending on the operating conditions (feed composition, temperature, and pressure) and on the purity requirements of the product gas, different processes can be used for the separation of $CO_2$ from natural or synthesis gas: i) (chemical or physical) absorption by a solvent, ii) pressure swing adsorption (PSA) on a solid adsorbent, iii) membrane separation, and iv) cryogenic separation. Global climate change, which is in part provoked by the $CO_2$ emissions of industrial installations, has revived interest in $CO_2$ separations[1] and has added a new constraint to these separation processes. While in former times the stream of extracted $CO_2$ was merely a waste stream that was vented to the atmosphere, the new challenge is to make the $CO_2$ waste stream ready for sequestration, which implies that is has to respond to quite stringent specifications in terms of purity. Moreover, as $CO_2$ has to be compressed to supercritical pressure for its transport and sequestration, separation processes that produce the $CO_2$ waste stream at high pressure are preferable because the cost of compression to the supercritical state is strongly reduced.

In this contribution, we focus on $CO_2$ separation by means of PSA. PSA processes are mainly used for the purification of $H_2$ from synthesis gas and for the separation of $CO_2$ and $CH_4$ in biogas or synthetic natural gas. However, current PSA processes are designed to achieve a high purity of the raffinate product, that is, $H_2$ and $CH_4$, respectively, but not of the $CO_2$ extract stream. Current PSA adsorbents (activated carbons or zeolites) may, therefore, not be the most suited materials for producing a $CO_2$ waste stream that is ready for sequestration, while at the same time minimizing the energy consumption of the process (the consumption of energy for the separation of $CO_2$ in turn produces $CO_2$-emissions unless the energy source is $CO_2$-neutral). Therefore, alternative $CO_2$ adsorbent materials are intensively researched.[2–5] One class of very promising $CO_2$ adsorbents are porous coordination polymers (PCPs) or porous metal organic frameworks (MOFs). These crystalline hybrid solids are a versatile class of compounds built up from an almost infinite combination of diverse inorganic subunits (single ions, clusters, chains, layers of 3p or transition metals, lanthanides…), connected through polytopic ligands (phosphonate, carboxylate, imidazolate, tetrazolate…) to define three-dimensional frameworks with pores of various dimensionality (1D to 3D), size (micro to meso), and shape. The variation of their chemical composition leads to numerous solids, some of which exhibit extremely high permanent porosity[6,7] (surface area and pore volume) or dynamic porosity[8,9] (ability of the pores to adapt to their content while the solid remains crystalline). Finally, the polarity and hydrophilicity of the surface of the pores can rather easily be tuned by systematic organic functionaliza-

[a] Dr. G. D. Pirngruber, Dr. L. Hamon
Department of Separation, Division of Separation and Catalysis
IFP Energies Nouvelles
B.P. 3, 69360 Solaize (France)
Fax: (+33)437 702 066
E-mail: gerhard.pirngruber@ifpen.fr

[b] Dr. S. Bourrelly, Dr. P. L. Llewellyn, Dr. E. Lenoir
Laboratoire Chimie Provence, UMR CNRS 6264
Université d'Aix-Marseille
13397 Marseille Cedex 20 (France)

[c] Dr. V. Guillerm, Dr. C. Serre, Dr. T. Devic
Institut Lavoisier, UMR CNRS 8180
Université de Versailles-Saint-Quentin-en-Yvelines
78035 Versailles (France)

Supporting Information for this article is available on the WWW under http://dx.doi.org/10.1002/cssc.201100716.

tion.[7,10–12] For these reasons, PCPs or MOFs are now considered as promising adsorbents for gas storage or separation. Nevertheless, in spite of the numerous studies dealing with the $CO_2$ adsorption properties of MOFs, only very few of them have analyzed in detail the application-related aspects.[13–15] It is, therefore, still difficult to assess the potential of this new family of materials for $CO_2$ separations by means of PSA. Such processes are semi-continuous cyclic processes. The cycle (see the Supporting Information) comprises an adsorption step at high pressure, which removes $CO_2$ and eventually other impurities from the feed gas. When the adsorbent has reached a certain $CO_2$ loading, feeding is discontinued, the column is depressurized, and $CO_2$ and coadsorbed impurities are desorbed at low pressure. To produce a very pure $CO_2$ extract, the adsorbent bed is purged with $CO_2$ before desorption. The $CO_2$ purge removes the coadsorbed impurities from the column. For this purpose, a part of the $CO_2$ extract is depressurized and recycled to the column. The amount of $CO_2$ that has to be recycled depends considerably on the selectivity of the adsorbent. Intrinsically, very selective adsorbents need very little purge to meet the purity requirement of the $CO_2$ extract ($>95\%$). Adsorbents of low selectivity either cannot meet the purity requirement at all or require a large amount of $CO_2$ to be recycled. The compression of the $CO_2$ recycle stream increases the energy consumption of the process, which is undesirable.

The PSA performance of new materials, such as MOFs, can be evaluated either experimentally in a lab-scale pilot or by means of numerical simulations. To yield representative results, even a lab-scale PSA pilot unit must have a considerable size ($>0.5\ m^3$) to reproduce heat effects correctly (vide infra). Such experiments are not feasible in a screening phase, for which a large number of adsorbents should be tested. Numerical simulations are easier to perform, but to yield precise results they require a large number of input parameters, which have to be acquired by performing extensive experimental measurements. Also, this procedure is too onerous for a broad initial screening phase. We, therefore, need simple, but pertinent criteria to select one or two materials for a more detailed evaluation.

These criteria are:[16]

1. The working capacity (or delta loading): It is defined as the difference of the adsorption capacity at high and low pressure. It is the amount of $CO_2$ that the adsorbent can take up during each adsorption cycle. The higher the working capacity, the higher the productivity, that is, the larger is the amount of feed that can be treated with a given amount of adsorbent in a given time. Productivity also depends on the adsorption kinetics, that is, on the mass transfer rate between gas phase and adsorbed phase, but mass transfer depends considerably on the shaping of adsorbents and is considered to be of secondary importance in an initial screening.

2. The selectivity for adsorption of $CO_2$ versus $CH_4$, CO, etc: A high selectivity is necessary to meet the stringent purity requirements of the $CO_2$ extract stream and to minimize the purge gas consumption.

3. The regenerability at pressures above 0.1 MPa: A higher desorption pressure reduces the energy consumption for the compression of the $CO_2$ extract to a supercritical state. We will, however, see that many applications leave little margin for increasing the desorption pressure above 1 bar because the $CO_2$ partial pressure in the feed is not very high.

4. The heat of adsorption: It should be as low as possible to avoid strong temperature excursions in the adsorbents bed, which degrade the quality of the separation. Yet, a low heat of adsorption of $CO_2$ often goes in pair with a low selectivity for the latter.

5. Stability under operating conditions: Although this parameter is obvious, it should be mentioned in the case of MOFs, as their stability, especially towards water[17,18] or acidic gases such as $H_2S$[19] have been shown to be strongly dependent on their chemical composition and structure.

In the present contribution, we analyze several MOF materials as PSA adsorbents with respect to the above-mentioned criteria. In an attempt to cover the large structural diversity of MOFs, we have chosen for this analysis (see the Supporting Information for structures):

1. Flexible 1D pore system MOF: MIL-53(Cr) or [Cr(OH)(bdc)] (bdc = 1,4-benzenedicarboxylate)[8]
2. Rigid small 1D pore system MOF: MIL-140(Zr)-A or [ZrO-(bdc)][20]
3. Rigid medium pore MOF: MIL-47(V) or [VO(bdc)][21]
4. Rigid, medium 3D pore system MOF with coordinatively unsaturated metal sites (CUS): Cu-btc (or HKUST-1) or $[Cu_3(btc)_2]$ (btc = 1,3,5-benzenetricarboxylate) [22]
5. Rigid large 3D pore system MOF with CUS: MIL-100(Cr) or $[Cr_3OX(btc)_2]$, X = OH, F.[23]

The target applications are the adsorption of $CO_2$ from syngas [for $H_2$ purification and for IGCC (integrated gasification combined cycle) systems] and the separation of $CO_2$ and $CH_4$ in biogas or synthetic natural gas. The above-mentioned MOF materials are compared with reference adsorbents, that is, zeolite NaX (13X) and an activated carbon, AC35, as well as with other MOF materials from the literature.

## Experimental Section

### Synthesis and activation

The solids were prepared under either hydrothermal [MIL-53(Cr),[8] MIL-47(V),[21] MIL-100(Cr)[24]] or solvothermal [Cu-btc,[25] MIL-140(Zr)-A[20]] conditions following the published procedures (see the Supporting Information for MIL-140(Zr)-A); experimental details are summarized in Table 1. All the syntheses were easily reproducible, and worked well on the gram (to few grams) scale. Whereas the use of 'green' solvents (water, alcohol) is beneficial, not only the synthesis but also the activation step should be considered. For example, the activation of MIL-47(V) and MIL-53(Cr) required an intermediate step, which consisted of the dispersion of the as-synthesized solid in a toxic solvent (*N*,*N*'-dimethylformamide) to remove the unreacted carboxylic acid entrapped in the pores. With the exception of MIL-47(V), all the solids were finally easily activated upon heating. For MIL-47(V), this step was sensitive to the amount of solid,[26] and complete activation should be checked carefully. The Brunauer–Emmett–Teller (BET) surface area and pore volume for the activated solids used in this study are summarized in Table 2.

  

**Table 1.** Reactants and synthesis conditions for the MOFs used in this study (bdc = 1,4-benzendicarboxylate; btc = 1,3,5-benzenetricarboxylate, DMF = *N*,*N*-dimethylformamide).

| MOF | Synthesis | | | | | | Activation | | | | |
|---|---|---|---|---|---|---|---|---|---|---|---|
| | | | | | | | Exchange | | | Calcination | |
| | Metal source | Ligand | Auxiliary reactant | Solvent | *T* [K] | *t* [h] | Solvent | *T* [K] | *t* [h] | *T* [K] | *t* [h] |
| MIL-53(Cr) | $Cr(NO_3)_3{\cdot}xH_2O$ | $H_2BDC$ | HF | $H_2O$ | 493 | 96 | DMF | 423 | 24 | 473 | 48 |
| MIL-140(Zr)-A | $ZrCl_4{\cdot}xH_2O$ | $H_2BDC$ | – | DMF | 493 | 24 | – | – | – | 473 | 24 |
| MIL-47(V) | $VCl_3$ | $H_2BDC$ | – | $H_2O$ | 473 | 72 | DMF | 423 | 24 | 523 | 48 |
| Cu-btc | $Cu(NO_3)_3{\cdot}3H_2O$ | $H_3BTC$ | – | $H_2O$/EtOH | 393 | 24 | – | – | – | 448 | 6 |
| MIL-100(Cr) | Cr | $H_3BTC$ | HF | $H_2O$ | 493 | 96 | $H_2O$ | 373 | 24 | 473 | 24 |

**Table 2.** Characteristics of the adsorbents used in this study.

| MOF | Pore shape | Pore size [nm] | $S_{BET}$ [$m^2\,g^{-1}$] | $V_{micro}$ [$cm^3\,g^{-1}$] | Porosity $cm^3\,g^{-1}$ | $\rho_{grain}$ [$g\,cm^{-3}$] | $\rho_{cryst}$ [$g\,cm^{-3}$] | $C_p$ [$J\,kg^{-1}\,K^{-1}$] |
|---|---|---|---|---|---|---|---|---|
| MIL-53(Cr) | channel | ≈0.7 | 1175 | 0.49 | 0.50 | 1.02 | 1.03 | n.d.[a] |
| MIL-140(Zr)-A | channel | ≈0.35 | 400 | 0.195 | 0.26 | 1.33 | 1.74 | n.d.[a] |
| MIL-47(V) | channel | ≈0.7 | 805 | 0.38 | 0.40 | 1.06 | 1.00 | 1066 |
| Cu-btc | cages | 1.0, 1.2 | 2200 | 0.81 | 0.65 | 0.80 | 0.88 | 920 |
| MIL-100(Cr) | cages | 2.5, 2.9 | 1790 | 0.78 | 0.58 | 0.82 | 0.74 | 1820 |
| AC35 | disordered | 0.5–1.3 | 1310 | 0.46 | 0.31 | 0.675 | – | 880 |
| NaX | cage | ≈1.0 | 820 | 0.34 | 0.49 | 1.45 | 1.42 | 900 |

[a] n.d. = not determined.

### Gravimetry

The adsorption isotherms of $CO_2$, $CH_4$, and CO were measured in a Rubotherm magnetic suspension balance at 303 K after degassing the samples at high temperature in vacuum (see the Supporting Information for details). The gravimetric measurements yield an excess adsorbed mass ($M_{excess}$), which was converted to the absolute adsorbed mass ($M_{abs}$) by means of Equation (1):

$$M_{abs} = M_{excess} + \rho_{gas} V_{micro} \quad (1)$$

where $\rho_{gas}$ is the gas density and $V_{micro}$ the micropore volume of the adsorbent [in the case of MIL-100(Cr), this is actually a mesopore volume]. The use of this correction implies that the volume of the adsorbed phase was considered to be equal to the micropore volume of the adsorbent. This assumption is questionable for large pore sizes, as in MIL-100(Cr).

### Adsorption microcalorimetry

The enthalpies of adsorption were obtained by using a manometric adsorption apparatus coupled with a Tian-Calvet type microcalorimeter.[27] Around 0.3 g of sample was used for these experiments. A point-by-point introduction adsorptive procedure was used to evaluate the amounts adsorbed and the pseudo-differential enthalpy of adsorption by means of the measured exothermic thermal effect associated with each dose.

### Heat capacities

The heat capacities ($C_p$) were measured in a C80 calorimeter from Setaram. A temperature ramp between an initial and a final temperature was imposed, and the heat flux between a cell containing the sample and an empty cell was measured. Integration of the heat flux produced the enthalpy change of the sample. The heat capacity was then calculated by using Equation (2).

$$C_p = \frac{\Delta H_{sample} - \Delta H_{blank}}{m^*(T_{final} - T_{initial})} \quad (2)$$

$\Delta H_{blank}$ corresponds to the enthalpy change measured in a blank experiment.

### Breakthrough measurements

A homemade breakthrough apparatus was used to measure the separation of $CO_2/CH_4$ and $CO_2/CH_4/CO$ mixtures. The adsorbent was placed inside a stainless steel column (MOFs in the form of powders, NaX as spheres of 500 μm, which contained 16 wt% binder material, AC35 as granulates). The samples were activated under He flow at an appropriate temperature (see the Supporting Information). After cooling down, the sample was pressurized under He flow. Then the feed mixture was injected through the column.

The measurements were carried out at 0.1, 0.5, and 1 MPa) at 303 K. Depending on the sample, the feed flow rate was adjusted between 1 and 8 NL/h. The feed composition was 50:50 (v/v) for the case of $CO_2/CH_4$ binary mixture and 70:15:15 for the $CO_2/CH_4/CO$ ternary mixture. The latter composition was close to the $CO_2/CH_4/CO$ ratio found in synthesis gas ex steam reforming of $CH_4$. In general, four experiments were carried out for each feed composition: i) a breakthrough curve He→feed; ii) a desorption curve feed→He; iii) a breakthrough curve on a column presaturated with $CO_2$, that is, $CO_2$→feed; and iv) a desorption curve feed→$CO_2$. Experiments (i) and (ii) allowed for calculating the adsorbed amounts of $CO_2$, $CH_4$, and CO by integration of the breakthrough curve (vide infra), but the so-called roll-up effect produced a high uncertainty for the adsorbed amount of $CH_4$ and CO. Presaturation of the column with $CO_2$ avoided the roll-up in the breakthrough curves of $CH_4$ and CO and, therefore, allowed for a better precision of the adsorbed amount of the weakly adsorbed components in experiments (iii) and (iv).

The absolute adsorbed quantity at equilibrium was calculated from the first moment of breakthrough curve ($\mu$), according to Equation (3):

$$q_i = \frac{C_i}{m_{ads}}\left(F\mu - V_{col} + \frac{m_{ads}}{\rho_{grain}}\right) \quad (3)$$

where $q_i$ is the absolute adsorbed amount of component i, $C_i$ the concentration in the gas phase, $m_{ads}$ the mass of the adsorbent, $F$ the total volumetric flow, $V_{col}$ the volume of the column, and $\rho_{grain}$ the grain density of the adsorbent. The first moment was calculated according to Equation (4):

  

$$\mu = \int \left(1 - \frac{F_i}{F_{i,0}}\right) dt \quad (4)$$

where $F_i$ is the flow rate of component i at the column outlet and $F_{i,0}$ the feed flow rate of component i. The first moment was corrected for the dead time of the setup, which was determined by means of a blank experiment.
The coadsorption selectivity was calculated using Equation (5):

$$S_{i,j} = \frac{q_i/q_j}{C_i/C_j} \quad (5)$$

For validating the breakthrough experiments with respect to the gravimetric measurements, we also recorded the breakthrough curves of pure $CO_2$. In the case of NaX and Cu-btc, the agreement with the gravimetric results was excellent. In the case of AC35, MIL-100(Cr), MIL-47(V), and MIL-140 A, the breakthrough curves underestimated the adsorbed quantity. This could be attributed to the difficulty of correctly activating these samples in a large column under inert gas flow, as compared to the use of vacuum on a considerably smaller amount of sample in the gravimetric experiments or to discrepancies between the batches used for both measurements.

### Water stability and coadsorption of $CO_2$ and $H_2O$

To evaluate the stability with respect to humidity, water adsorption–desorption cycling at 298 K was investigated. Experiments were carried out by using a gravimetric device (Q5000SA, TA Instruments) that combined a high-sensitivity thermobalance and a humidity control chamber. The sample mass used for these experiments was around 10 mg. The samples were activated at 353 K for 4 h under inert gas flow ($N_2$) directly inside the thermobalance. Five water adsorption–desorption cycles were performed from 5 to 95% relative humidity at 298 K without any thermal regeneration between each run.

The coadsorption of $CO_2$ and $H_2O$ was tested in a breakthrough apparatus similar to the one described in the previous section. The adsorbent (1–2 g) was filled into a column of 10 cm length and 0.7 cm diameter. $N_2$ was used as "inert gas" instead of He. Three concentration steps were carried out: v) a step from dry $N_2$ to dry $CO_2$; vi) a step from $N_2$ to $CO_2$, both saturated with $H_2O$; and vii) a step from $N_2$ saturated with $H_2O$ to $CO_2$ saturated with $H_2O$. For experiments of type (vii), the adsorbent was contacted with the humid $N_2$ stream for different times before switching to $CO_2$. The experiments were carried out at atmospheric pressure and 303 K. The humidity level was close to 100%. The $H_2O$ and $CO_2$ concentration at the column effluent were analyzed by using an IR detector.

## Results

### Characterization of the samples

Some important physicochemical characteristics of the adsorbents, that is, pore size and shape, surface area, pore volume, grain density, and heat capacity, are compiled in Table 2. In terms of pore size, the samples can be classified in three categories. MIL-140(Zr)-A has a pore size that is close to the dimensions of the molecules that we want to separate, and might, therefore, exhibit molecular sieving properties. MIL-53(Cr)/47(V), Cu-btc, AC35, and NaX have medium pore sizes in the range of 0.7–1.0 nm. MIL-100(Cr) has microporous windows (0.5–1 nm) leading to mesoporous cages (pore size > 2 nm). We recall that the confinement in a small pore reinforces the van der Waals interactions between adsorbent and adsorbate.

The micropore volume of the adsorbents determines the maximum adsorption that can be reached at saturation of the pores, that is, at high pressure. The order of micropore volumes in $cm^3 g^{-1}$ is MIL-100(Cr) ≈ Cu-btc > MIL-53(Cr)/47(V), AC35 > NaX > MIL-140 A. However, to determine the dimensions of an adsorption column, the adsorption capacity per volume of adsorbent is more relevant than the adsorption capacity per mass. The capacity per mass is converted into a capacity per volume by multiplying with the grain density of the adsorbent. The grain density can either be calculated from the crystallographic structure or be measured experimentally (see the Supporting Information). Table 2 shows that the theoretical and experimental densities are in very good agreement [with the exception of MIL-140(Zr)-A: The skeletal density of MIL-140(Zr)-A is determined from its buoyancy in He; if adsorption of He on the sample is non-negligible the skeletal density and, as a consequence, also the grain density are underestimated]. MIL-140(Zr)-A and NaX are the densest samples of the series, MIL-100(Cr) and AC35 have the lowest densities. Multiplication of the pore volume in $cm^3 g^{-1}$ with the grain density gives the porosity (pore volume/grain volume). MIL-100(Cr) and Cu-btc are on top of the porosity ranking, AC35 and MIL-140(Zr)-A on the bottom.

The heat capacities of some of the samples are also included in Table 2; they will be used to calculate the temperature increase upon adiabatic adsorption. With the exception of MIL-100(Cr), which has a very high heat capacity, the $C_p$ values of MOFs are close to those of zeolites and activated carbons.[28–30]

### Adsorption isotherms and heats of adsorption

The adsorption isotherms of $CO_2$ on the samples of Table 2 (see the Supporting Information for the isotherms of $CH_4$ and CO) are shown in Figure 1. The absolute adsorbed amount is expressed in moles per adsorbent volume. At 5 bar, the $CO_2$ adsorption capacity per volume decreases in the order NaX > Cu-btc > MIL-100(Cr) ≈ MIL-47(V) > MIL-53(Cr) > MIL-140(Zr)-A ≈ AC35. MIL-140(Zr)-A and AC35 are at the bottom of the ranking because they are rather apolar adsorbents and, on top of that, they have a low porosity. We will come back to Figure 1 when discussing the application-related aspects. From a fundamental point of view it is more interesting to plot the isotherms as density of the adsorbed phase vs. density of the gas phase (Figure 2). The density in the adsorbed phase is the (absolute) adsorbed amount per micropore volume [the change of micropore volume of MIL-53(Cr) associated with its structural flexibility was not taken into account[31]]. Such a plot illustrates how adsorption concentrates the molecules compared to the gas phase and allows comparing the affinity between adsorbent and adsorbate, without interference of effect of the pore volume on the adsorption capacity.

  

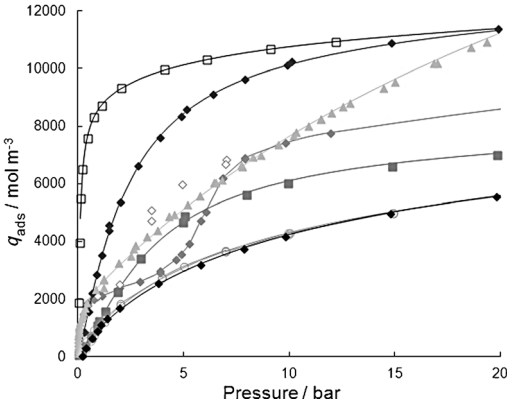


**Figure 1.** Adsorption isotherms of $CO_2$ at 303 K. $q_{ads}$ is the absolute adsorbed amount in mol per volume of adsorbent. ◆: MIL-53(Cr) adsorption, ◇: MIL-53(Cr) desorption, ■: MIL-47(V), ○: MIL-140(Zr)-A, ◆ Cu-btc, ▲: MIL-100(Cr), ◆: AC35, □: NaX.

NaX has by far the highest affinity for $CO_2$ (Figure 2a) due to the strong interaction of the quadrupole moment of $CO_2$ with the electric field exerted by the extra-framework cations of NaX. At low gas phase density, MIL-100(Cr) and MIL-53(Cr) follow NaX in the order of affinities for $CO_2$. MIL-100(Cr) interacts strongly with $CO_2$ through the Cr CUS,[32] but once these very strong adsorption sites are occupied, the affinity of MIL-100(Cr) for $CO_2$ is quite low. Because of the large pore size, confinement effects do not enhance the adsorption of $CO_2$, and its isotherm drops below that of Cu-btc and MIL-47(V). MIL-53(Cr) interacts with $CO_2$ through the OH-groups in the Cr–OH–Cr-chain, with a stronger donor (OH)–acceptor ($CO_2$) interaction in the NP form (0.3–6 bar) than in the large pore (LP) form ($P > 6$ bar).[33]

The differential enthalpies of adsorption, calculated from calorimetry measurements (Figure 3a), confirm that at very low pressure the adsorption of $CO_2$ is strongest on MIL-100(Cr) and NaX. For both solids, the enthalpy curve decreases with adsorption, revealing that the surfaces are energetically heterogeneous. The peak in the enthalpy curve of MIL-53(Cr) above 0.3 bar occurs when the structure transforms to the NP form.[34]

Cu-btc contains CUS, similar to MIL-100(Cr), but their interaction with $CO_2$ is considerably weaker than in the case of MIL-100(Cr), presumably because $Cu^{2+}$ is fairly stable in a square planar coordination. As a consequence, the adsorption enthalpy is only $-30$ kJ mol$^{-1}$.[35] MIL-140(Zr)-A's heat of adsorption is similar to Cu-btc's, but its adsorbed phase density is considerably lower. On the contrary, MIL-47(V) exhibits a fairly low enthalpy ($-21$ kJ mol$^{-1}$ during the initial stages of adsorption, increasing to $-25$ kJ mol$^{-1}$ at higher coverage), but according to Figure 2 its $CO_2$ affinity is similar to Cu-btc's. The data demonstrate that the adsorbed phase density is not uniquely governed by enthalpic effects. The density of adsorption sites and other entropic effects also come into play.

Methane does not possess any permanent dipole or quadrupole moment. Therefore, its interactions with an adsorbent are generally weaker than those of $CO_2$. Whilst its polarizability

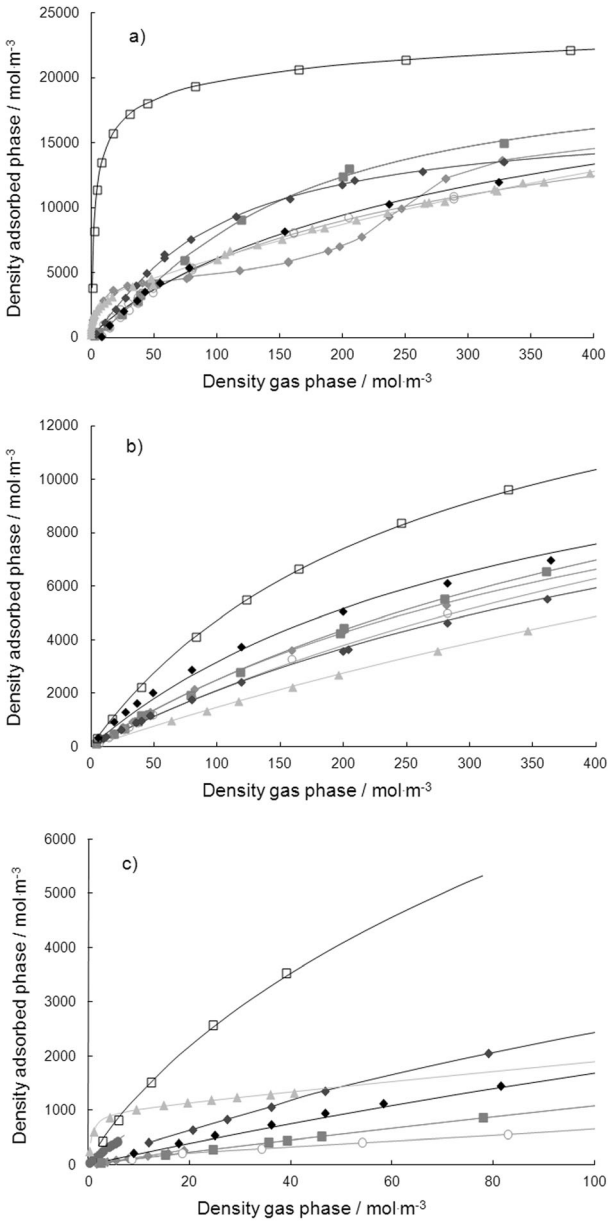


**Figure 2.** Adsorption isotherms of a) $CO_2$, b) $CH_4$, and c) CO at 303 K. ◆: MIL-53(Cr) adsorption, ■: MIL-47(V), ◆ Cu-btc, ▲: MIL-100(Cr), ◆: AC35, □: NaX, ○: MIL-140(Zr)-A.

(which is similar to that of $CO_2$) allows methane to interact with specific surface sites, confinement effects due to pore size can be just as important. This is well highlighted in the initial enthalpies of adsorption here (Figure 3b), for which an order of MIL-47(V) < MIL-53(Cr) < MIL-100(Cr) < NaX < Cu-btc < AC35 < MIL-140(Zr)-A is observed. The medium pore size MOFs, MIL-47(V) and MIL-53(Cr), show the lowest enthalpies, with the latter having a slightly larger enthalpy due to the $-$OH group. MIL-100(Cr) and Cu-btc exhibit slightly higher enthalpies due to the CUS, whereas the very-small-pore samples, AC35 and MIL-140(Zr)-A, show the highest enthalpies due to the confinement effect within very small pores close to the size of the methane molecule itself (the kinetic diameter of $CH_4$ is 0.38 nm). The zeolite NaX does not stand out in terms

  

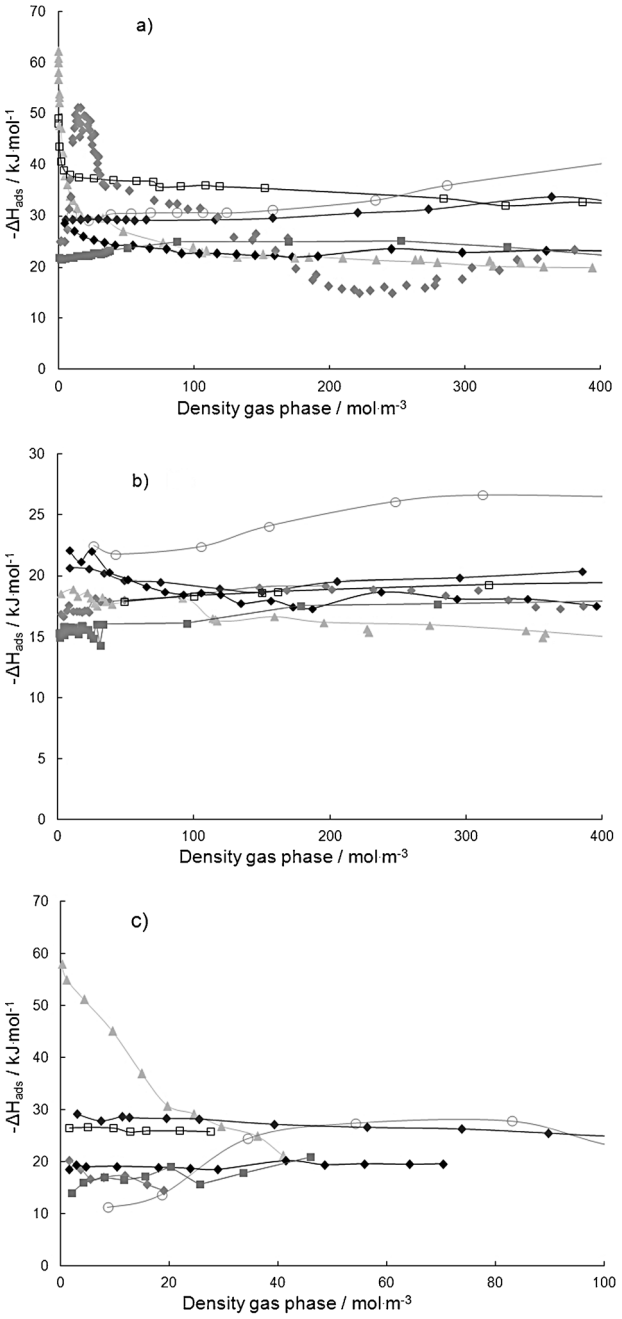


**Figure 3.** Differential enthalpies of adsorption of a) $CO_2$, b) $CH_4$, and c) CO. ◆: MIL-53(Cr) adsorption, □: NaX, ◆ Cu-btc, ■: MIL-47(V), ▲: MIL-100(Cr), ○: MIL-140(Zr)-A, ◆: AC35.

of its enthalpy, but has by far the highest adsorbed phase density (Figure 2b). This is tentatively attributed to a higher density of adsorption sites.

Finally, Figure 2c compares the low pressure isotherms of CO on some of the adsorbents. The trends are different from $CH_4$. The highest CO density is still found in NaX because NaX strongly polarizes CO.[36] The CUS of MIL-100(Cr) also strongly adsorb CO through a Lewis-acid–base interaction,[32] which is confirmed by high enthalpies of adsorption: around $-59\ kJ\,mol^{-1}$ for the first adsorbed molecules followed by a strong decrease to $-30\ kJ\,mol^{-1}$ (Figure 3c). As already observed for $CO_2$, the CUS–CO interaction in Cu-btc is significantly weaker. The hypsochromic shift of the CO stretching frequency is considerably smaller,[25] and the adsorption enthalpy is only $-30\ kJ\,mol^{-1}$ even at low adsorbate loadings. The apolar adsorbents MIL-140(Zr)-A, AC35, and MIL-47(V) have the lowest affinity for CO. The interaction of CO with the OH-groups of MIL-53(Cr) is also quite weak because of the very weak acidity of this solid.[33]

### Breakthrough experiments: Separation of $CO_2/CH_4$

The breakthrough curves of equimolar $CO_2/CH_4$ mixtures at 5 bar over the adsorbents NaX, AC35, Cu-btc, MIL-100(Cr), MIL-47(V), and MIL-140(Zr)-A are shown in Figure 4. The breakthrough curves were recorded by using columns of different lengths and different flow rates (see the Supporting Information). For comparison, we present the time axis as the cumulated feed volume divided by the column volume. Such a comparison is only qualitative, as the packing density of the columns was not necessarily optimal in all cases.

The time lag between the breakthrough of $CH_4$ and $CO_2$ gives an indication of the quality of separation. Simple inspection of the curves shows that the quality of separation decreases in the order $NaX > Cu\text{-}btc > MIL\text{-}100(Cr) > MIL\text{-}47(V) \approx AC35 \gg MIL\text{-}140(Zr)\text{-}A$. All the breakthrough curves of $CH_4$ exhibit a so-called roll-up effect, that is, the flow rate of $CH_4$ at the column exit temporarily exceeds the feed flow rate. The roll-up can be explained as follows: The concentration front of $CH_4$ advances faster through the column than the concentration front of $CO_2$. Therefore, the outlet end of the column is initially only in contact with $CH_4$. The time of first breakthrough of $CH_4$ is a measure of the affinity of the adsorbent for pure $CH_4$. As the concentration front of $CO_2$ advances further through the column, $CO_2$ replaces $CH_4$ that was initially adsorbed, that is, $CH_4$ is desorbed by incoming $CO_2$. This leads to the roll-up. The amplitude of the roll-up is a measure of the competition between $CO_2$ and $CH_4$ for adsorption sites. Its amplitude is high when a large amount of $CH_4$ is rapidly replaced by incoming $CO_2$. An adsorbent may be selective because it intrinsically adsorbs very little $CH_4$ (early breakthrough of $CH_4$, weak roll-up), strongly prefers $CO_2$ over $CH_4$, in spite of a fairly strong interaction with $CH_4$ (late breakthrough of $CH_4$, strong roll-up), or by a combination of both effects.

In the breakthrough curves of NaX, Cu-btc, and MIL-100(Cr), an additional peak appears in the $CH_4$ roll-up, just before $CO_2$ breaks through the column. This peak is due to the temperature wave that accompanies the concentration front of $CO_2$. The adsorption of $CO_2$ is more exothermic than that of $CH_4$, which leads to a temporary temperature increase in the bed. This temperature increase triggers further desorption of $CH_4$ and leads to the additional peak in the roll-up. Note that the effect is hardly visible in the case of MIL-47(V), MIL-140(Zr)-A, and AC35, in agreement with their lower adsorption enthalpy for $CO_2$.

In the integration of the breakthrough curve, the roll-up, that is, the area above $F/F_0 = 1$ ($F$ is the flow rate at the column outlet and $F_0$ the feed flow rate), is counted as a negative ad-

  

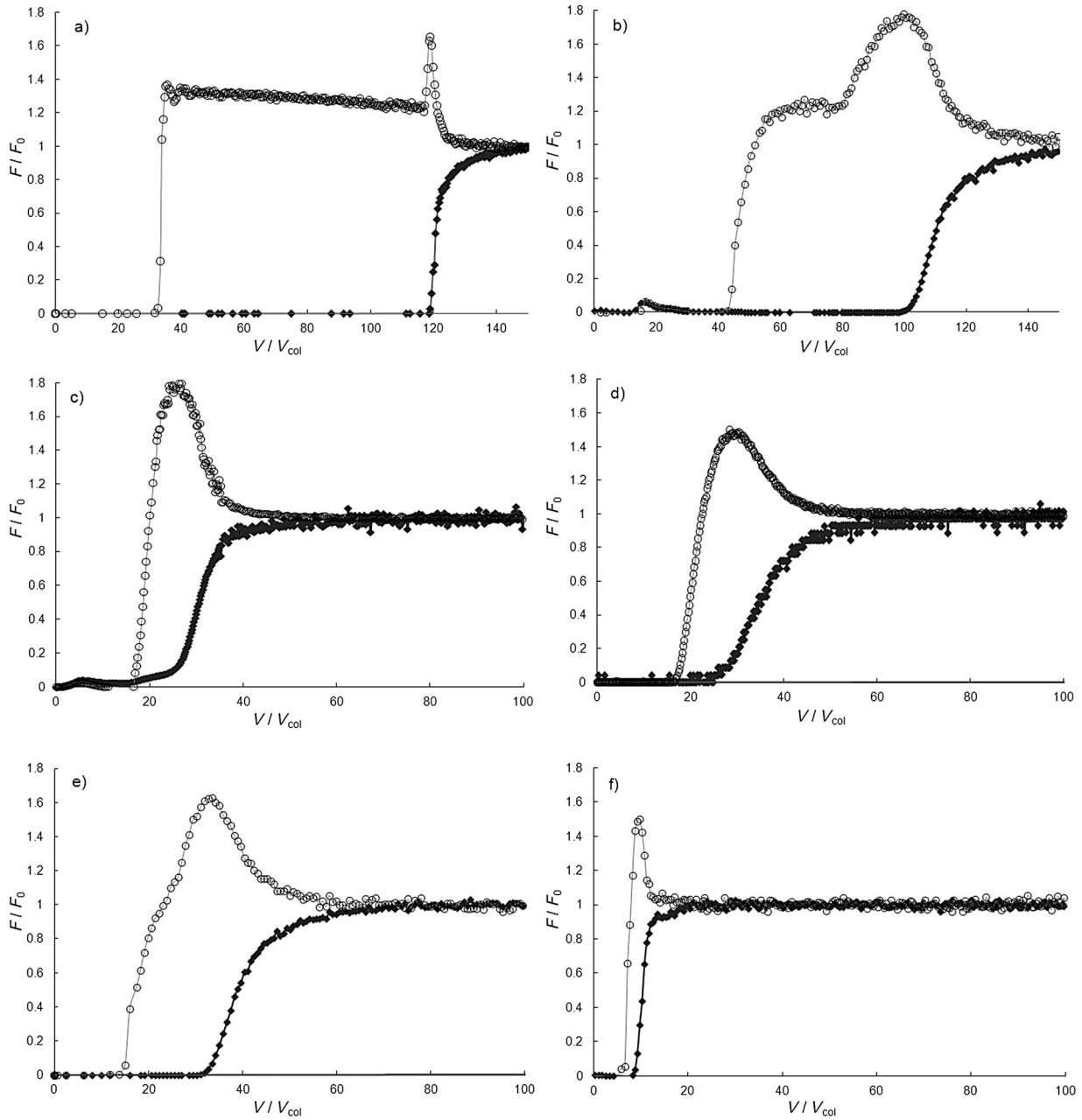


**Figure 4.** Breakthrough curves of binary mixtures of $CO_2$ (◆)/$CH_4$ (○) (50:50 v/v) over a) NaX, b) Cu-btc, c) MIL-47(V), d) AC35, e) MIL-100(Cr) and f) MIL-140(Zr)-A at 5 bar and 303 K.

sorbed amount. Therefore, it is difficult to estimate the final adsorbed amount of $CH_4$ directly from the breakthrough curve. The desorption curve shows more clearly the amount of $CH_4$ that is still adsorbed when the whole column is equilibrated with the feed (i.e., at the end of the breakthrough curve). Figure 5 compares the desorption curves of the adsorbents NaX and MIL-100(Cr). The huge peak in the desorption curve at $t<0$ is due to the purging of the dead volume of the system. The true desorption starts at $t>0$. We point out two important observations in Figure 5: The amount of $CH_4$ desorbed from NaX is extremely small, that is, very little $CH_4$ was coadsorbed on NaX after complete breakthrough of the feed. Secondly, the desorption of $CO_2$ from the NaX column is difficult. The desorption curves are spread out over a very long time period. After a desorption time equal to the breakthrough time, only 30% of the initially adsorbed amount has been desorbed. In the case of MIL-100(Cr), on the other hand, desorption is considerably faster. At desorption time = breakthrough time, 50% of the $CO_2$ has been desorbed, but we also determined that a larger amount of $CH_4$ was coadsorbed in the column.

The $CO_2/CH_4$ selectivity was calculated from Equation (5): The adsorbed amount of $CH_4$ was calculated by taking the average obtained from experiments (i)–(iv) described in the experimental section. The average was weighted according to the accuracy of each data point. In most cases, only the de-

  

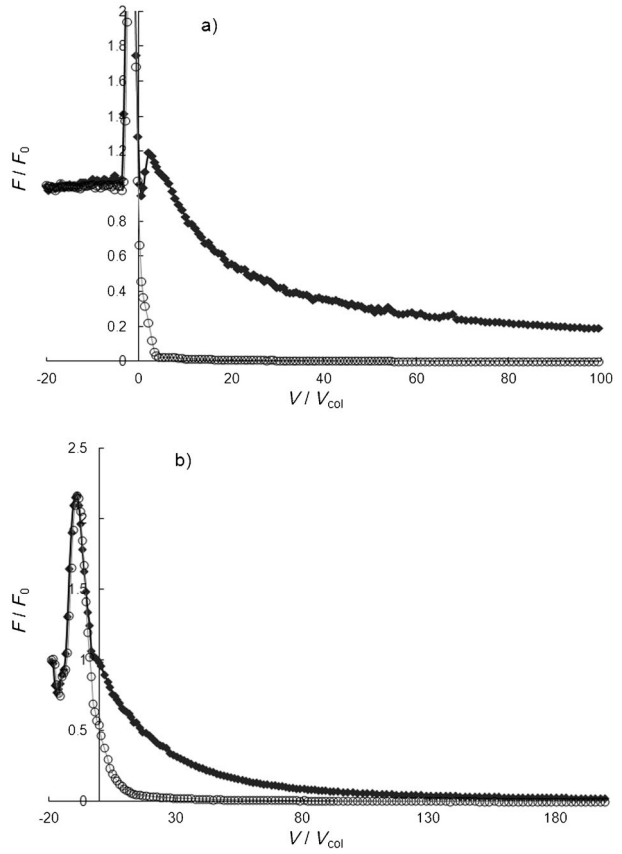


**Figure 5.** Isothermal desorption by He purge of a column equilibrated with a 50:50 (v/v) mixture of $CO_2$ (◆)/$CH_4$ (○) over a) NaX and b) MIL-100-Cr at 5 bar and 303 K.

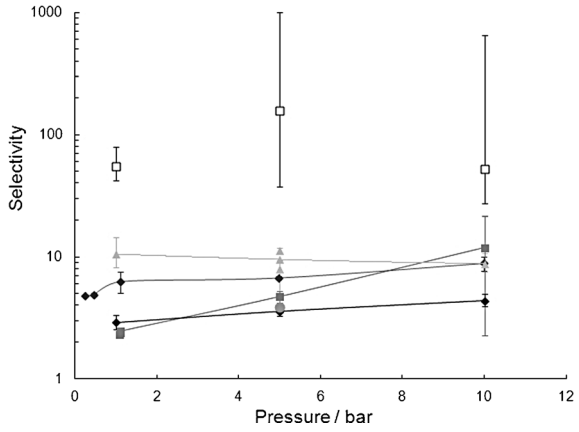


**Figure 6.** $CO_2/CH_4$ selectivity as a function of total pressure, as calculated from the breakthrough experiments. Error bars are indicated. □: NaX, ◆ Cu-btc, ▲: MIL-100(Cr), ■: MIL-47(V), ●: MIL-140(Zr)-A, ◆: AC35.

sorption experiment and the breakthrough curve on a presaturated column were used for calculating the average. Figure 6 compares the $CO_2/CH_4$ selectivity as a function of pressure for the five rigid adsorbents. NaX is clearly the most selective adsorbent. Thanks to the strong interaction of $CO_2$ with the coordinatively unsaturated $Cr^{3+}$ sites, MIL-100(Cr) is also quite selective (roughly constant selectivity of 10). Cu-btc has a smaller preference for $CO_2$ than MIL-100(Cr) because the CUS sites of Cu-btc interact more weakly with $CO_2$ than those of MIL-100(Cr). MIL-47(V) is not very selective at low pressure, but its selectivity strongly increases with pressure. This might be related to its adsorption enthalpy profile, which indicates that the affinity of MIL-47(V) for $CO_2$ increases with pressure. Finally, the selectivity of the apolar small pore MOF MIL-140(Zr)-A is similar to that of AC35.

### Breakthrough experiments: Separation of $CO_2/CH_4/CO$

The breakthrough curves of ternary $CO_2/CH_4/CO$ mixtures over NaX, AC35, Cu-btc, MIL-100(Cr), MIL-47(V), and MIL-140(Zr)-A are compared in Figure 7. As in the case of the binary mixtures, a simple inspection of the curves gives an indication of the quality of the separation. We find the order NaX > Cu-btc > MIL-47(V) ≈ AC35 > MIL-100(Cr) ≫ MIL-140(Zr)-A. MIL-100(Cr) performs less well in the ternary mixture than in the binary $CO_2/CH_4$ separation because of its stronger interaction with CO. We can also observe an interesting trend in the order of elution of CO vs. $CH_4$. Apolar adsorbents, such as activated carbons or MIL-47(V) and MIL-140(Zr)-A, elute in the order of the boiling points (or critical temperatures) of the three compounds, that is, $CO < CH_4 < CO_2$. In the case of Cu-btc, specific interactions of CO with the CUS compensate the stronger van der Waals interaction of $CH_4$, and the two compounds elute almost simultaneously from the column. MIL-100(Cr), similar to NaX, however, elutes $CH_4$ before CO because of the strong interaction of CO with CUS (or cations for NaX). At higher pressures (10–15 bar), as the role of CUS decreases, CO and $CH_4$ elute simultaneously over MIL-100(Cr) (not shown). In the case of NaX, the higher polarizability of CO compared to $CH_4$ enhances its interaction with the strong electric field of NaX.

The adsorbed quantities of $CH_4$ and CO at the end of the breakthrough curves (in equilibrium) are within the error margin of the experiments; hence, we cannot calculate reliable selectivity values, but we can state that the selectivities of the tested MOFs and NaX are rather high.

### Water stability

Synthesis gas or biogas are usually dried before entering the PSA unit, but the gas still contains some residual humidity. In PSA units, the residual humidity is usually adsorbed by a guard layer of silica gel or alumina, and under normal process operating conditions, very little $H_2O$ should come in contact with the $CO_2$ adsorbent. Nevertheless, temporary breakthroughs of $H_2O$ into the $CO_2$ adsorbent bed are always possible. As PSA adsorbents are meant to last for decades, it is important to evaluate the effect of $H_2O$ not only on the adsorption of $CO_2$, but also on the structural stability of the adsorbent. As already mentioned, the stability of MOFs toward water is highly dependent on their composition.[17,37,38] Whereas a Zn-carboxylate such as the archetypical MOF-5 is destroyed in the presence of humidity,[17] the Zr terephthalate UiO-66 (or $[Zr_6(OH)_4O_4(bdc)_{12}]$)[39] is stable in boiling water. The stability towards water can, in a first approach, be roughly correlated with the

  

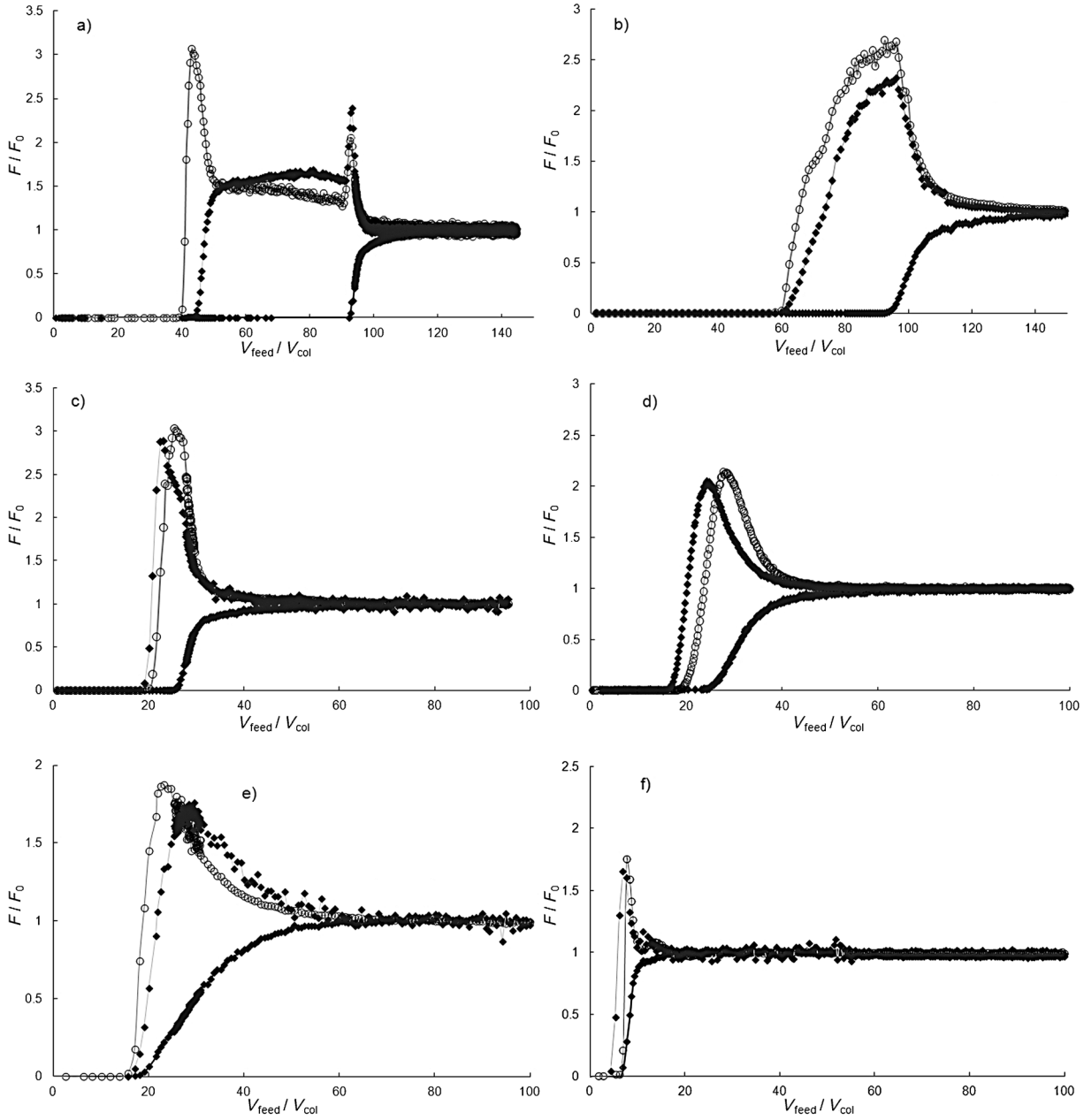


**Figure 7.** Breakthrough curves of 70:15:15 $CO_2$(—◆—)/$CH_4$(○)/CO(—◆—) mixtures at 5 bar and 303 K over a) NaX, b) Cu-btc, c) MIL-47(V), d) AC35, e) MIL-100(Cr), and f) .

strength of the metal (M)—carboxylate bond, leading to a higher stability for the highly charged cations ($M^{3+}$, $M^{4+}$). With the noticeable exception of MIL-47,[40] all the solids selected here are thus rather stable towards moisture.

A simple manner to follow the stability of these materials is to perform water adsorption–desorption cycling experiments. Such experiments can be seen in the Supporting Information for MIL-100(Cr) and Cu-btc. In the case of the MIL-100, the three isotherm cycles overlap, showing the full stability of this sample under these conditions. In the case of Cu-btc, there is a notable decrease in uptake with each cycle. This result can be understood with respect to a recent solid-state NMR study, which followed the structure of Cu-btc upon exposure to water.[41] The structure was shown to be stable when a small amount of water (0.5 molar equivalents with respect to Cu) was absorbed, but decomposition occurred at higher water contents.

The coadsorption of $CO_2$ and $H_2O$ was evaluated for Cu-btc and MIL-100(Cr). In both cases, the $CO_2$ adsorption capacity dropped only very little when performing a breakthrough experiment [experiment (vi), see Experimental] with a humid feed. However, breakthrough of water was not observed in these experiments, because the amount of water in the feed was not sufficient to saturate the whole adsorption column. The water adsorption front remained at the column inlet, which explains why little change in the adsorption capacity of

  

$CO_2$ was observed. When cycling between adsorption of humid $CO_2$ and desorption with dry $N_2$, a small, but continuous drop of the adsorption capacity was observed from one cycle to another because the water concentration front advanced further through the bed at each cycle. We therefore tried to presaturate the column with $H_2O$ for different times before switching to $CO_2$ [experiment (vii), see Experimental]. After presaturation for several hours, a clear drop in the adsorption capacity for $CO_2$ was observed, and the adsorption capacity dropped to zero after presaturation for several days (see Table 3). That implies that $CO_2$ cannot compete with $H_2O$ for adsorption sites at the high humidity level used in our experiments. $H_2O$ completely inhibits the adsorption of $CO_2$ on Cu-btc and MIL-100(Cr). Our data confirm recent experimental results by LeVan and coworkers on CPO-27(Ni) and Cu-btc,[42] which also show a strong inhibition of $CO_2$ adsorption by $H_2O$. Molecular modeling studies had suggested a beneficial effect of $H_2O$ on the $CO_2$ adsorption, but the effect is weak and only observed at very low humidity levels. For MOFs with open metal sites, it is, therefore, as important as for zeolite NaX to avoid contact of the adsorbent layer with $H_2O$ in the feed because $H_2O$ will deactivate the adsorbent.

In the case of Cu-btc, we further observed that exposure to $H_2O$ followed by thermal regeneration of the sample led to a drop of the adsorption capacity, in agreement with its limited stability when exposed to water.

## Discussion

### Prediction of coadsorption: Theory and experiment

The two most important selection criteria for $CO_2$ adsorbents are the working capacity and the selectivity. The working capacity determines the size of a $CO_2$ adsorption vessel, whereas purity, recovery of $CO_2$, and the purge gas consumption mainly depend on the so-called separation factor. The separation factor (SF) is defined as the ratio of delta loadings ($\Delta q$) of $CO_2$ and of the "impurities" $CH_4$ and CO [Eq. (6)]. The separation factor is an effective selectivity under the cyclic conditions of the PSA process.

$$SF = \frac{\Delta q_{CO_2}}{\Delta q_{impurities}} \cdot \frac{C_{impurities}}{C_{CO_2}} \qquad (6)$$

For an experimental determination of working capacity and separation factor, two breakthrough curves have to be measured: One under the conditions of adsorption, that is, at feed composition and feed pressure, and one under the conditions of desorption. In our case, we want to desorb pure $CO_2$ at 1 bar. The drawback of the experimental determination is that a breakthrough curve has to be measured for each feed composition and feed pressure that we want to test, which is experimentally quite demanding. Calculating $\Delta q$ and SFs from a coadsorption model would be more convenient because it allows us to play with the conditions of adsorption and desorption at our will. One has to verify, however, that the results from the model are in agreement with the experimental data.

Ideal adsorbed solution theory (IAST) was used to predict coadsorption from the single component isotherms. The single component excess isotherms of $CO_2$, $CH_4$, and CO were fitted by a single or dual site Langmuir–Freundlich isotherm (see the Supporting Information). The excess coadsorption was then calculated from IAST, and the absolute coadsorbed amounts were obtained by adding the contribution from the gas phase density, as in Equation (1). IAST predicts very well the experimental selectivities for Cu-btc,[43] MIL-140(Zr)-A and NaX. In the case of AC35 and MIL-47(V), IAST underestimates the measured selectivities, in particular at higher pressure, but qualitatively reproduces the experimentally observed increase of selectivity with pressure. IAST performs least well for MIL-100(Cr), for which it strongly overestimates the $CO_2/CH_4$ selectivity at low pressure. Agreement with experiment becomes better at higher pressure and the order of elution of CO vs. $CH_4$ is correctly predicted. The deviation of MIL-100(Cr) from IAS theory is not surprising as the strong dual-site adsorption behavior of MIL-100(Cr) is, in principle, incompatible with the assumption of an ideal adsorbed solution.

The plots of separation factor vs. working capacity obtained from the breakthrough experiments and the IAST calculations are compared in Figure 8. Although quantitative agreement is not perfect, the general trends are well reproduced. In both plots, NaX is clearly identified as the most selective adsorbent, Cu-btc as the most capacitive one, and AC35 and MIL-140(Zr)-A as the least attractive materials. We may conclude that IAST, in spite of some shortcomings, is well suited for categorizing adsorbents in a screening phase. In the following section we, therefore, use IAST for screening the performance of MOF adsorbents in several industrial applications by means of the criteria working capacity and separation factor.

**Table 3.** Adsorption capacity for a $CO_2$ feed saturated with $H_2O$, after presaturation of the adsorbent with humid $N_2$ for different times ($T = 303$ K, pressure 1 bar).

| MOF | Presaturation time [h] | Prefed $H_2O$ [mol $kg_{sorbent}^{-1}$] | Capacity $CO_2$ [mol $kg^{-1}$] | Relative capacity [%] |
|---|---|---|---|---|
| MIL-100(Cr) | 0 | – | 1.42 | 100 |
| | 6 | 3.24 | 0.71 | 50 |
| | 48 | 25.92 | 0 | 0 |
| Cu-btc | 0 | – | 2.5 | 100 |
| | 7 | 5.05 | 0.8 | 30 |
| | 21 | 15.15 | 0.4 | 15 |

### Estimation of isothermal working capacity and separation factors

We estimated the isothermal working capacity and separation factor of the adsorbents for three different applications: i) the separation of $CO_2$ and $CH_4$ in biogas (or synthetic natural gas), ii) the purification of $H_2$ with $CO_2$ capture, and iii) $CO_2$ capture in IGCC plants. The somewhat idealized feed compositions and pressures used in our analysis are compiled in Table 4. Biogas has a close to 50:50 composition of

  

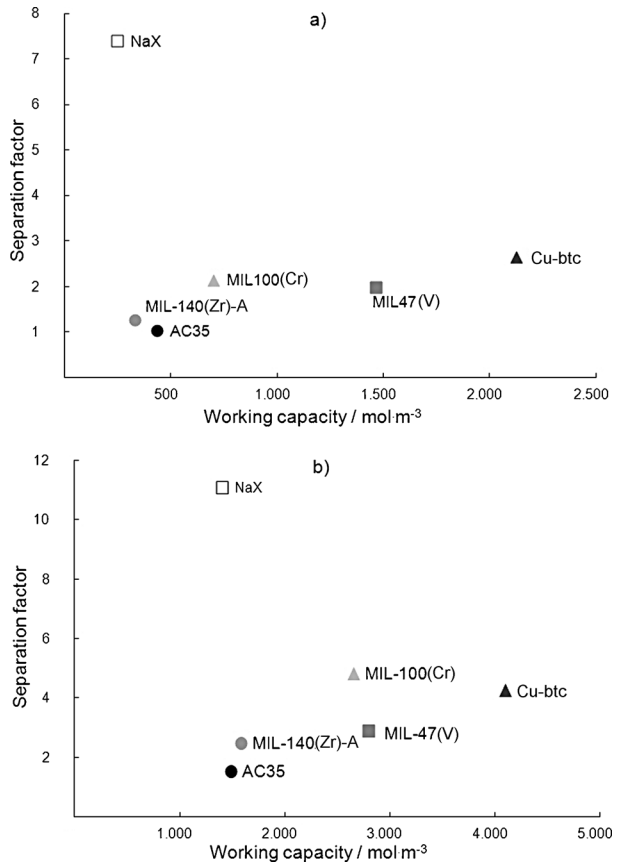


**Figure 8.** Separation factor vs. working capacity for the separation of a 50:50 mixture CO2/CH4 at 5 bar, with desorption of $CO_2$ at 1 bar. a) Experimental values obtained from breakthrough curves, b) values calculated from an IAST model.

**Table 4.** Total pressure, feed composition, and partial pressure of $CO_2$ for the different applications considered in this study.

| Application | Total pressure [bar] | Feed composition [mol%] | | | | $p_{CO_2}$ [bar] |
|---|---|---|---|---|---|---|
| | | $H_2$ | $CO_2$ | $CH_4$ | CO | |
| $H_2$ purification | 22 | 75 | 16 | 4.5 | 4.5 | 3.5 |
| IGCC (1) | 28 | 55 | 40 | – | 2.5 | 11.1 |
| IGCC (2) | 57 | 55 | 40 | – | 2.5 | 22.9 |
| Biogas | 10 | – | 50 | 50 | – | 5.0 |

$CO_2/CH_4$ and contains little or no CO. Biogas is usually delivered at low pressure and needs to be compressed before the PSA unit. Compression to 10 bar is convenient for the subsequent injection of $CH_4$ into a local gas grid. In the case of $H_2$ purification, the feed corresponds to a synthesis gas used for high-temperature water gas shift reaction. For IGCC, a typical syngas composition produced by the high temperature gasification of coal was used. IGCC syngas does not contain $CH_4$, the relevant separation is $CO_2$/CO. The adsorption of $H_2$ was always supposed to be negligible, in agreement with the numerous studies on hydrogen storage in MOFs, which concluded that, although these solids could present high capacities at low temperature, the amount of $H_2$ adsorbed around room temperature is always very limited.[44–46] Two different pressure levels were chosen for IGCC, corresponding to different gasification technologies. Desorption conditions were always 1 bar and pure $CO_2$. In the case of the high-pressure IGCC application, we tested the effect of a higher desorption pressure.

### Biogas separation

The plot of separation factor vs. the working capacity for the case of the biogas separation, which includes the MOFs tested in this study and some representative literature data, is shown in Figure 9.[13,47–51] The adsorbents with the highest working capacity are Cu-btc, PCN-11, and PCN-16. All three are Cu-polycarboxylate MOFs with coordinatively unsaturated metal sites, but with different pore structures.[52] PCN-11 and PCN-16 have a slightly higher working capacity than Cu-btc because their porosity is higher (0.76 for PCN-16 and 0.68 $cm^3 g^{-1}$ for PCN-11 vs. 0.65 $cm^3 g^{-1}$ for Cu-btc). The high working capacity of the three Cu-based MOFs suggests that coordinatively unsaturated Cu-sites and microporosity offer the best compromise in terms of $CO_2$ affinity. Their interaction with $CO_2$ is sufficiently strong to fill a large portion of the pore volume at $p_{CO_2} = 5$ bar, while allowing at the same time an "easy" regeneration at 1 bar (see Figure 1).

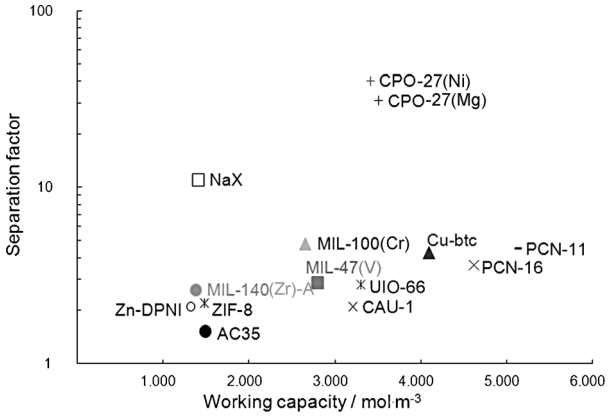


**Figure 9.** Separation factor vs. working capacity for biogas separation (50:50 mixture $CO_2/CH_4$). Adsorption pressure 10 bar, desorption pressure 1 bar.

The most selective adsorbents, according to Figure 9, are CPO-27[53] (or [$M_2$(dobdc)], dobdc = dioxoterephthalate, M = Ni, Mg…) MOFs. Similar to MIL-100(Cr), the CPO-27 MOFs have a strong dual site behavior. We have seen in the previous section that IAST is not very reliable for predicting the selectivity of such systems. Experimental confirmation of the very promising separation factors is, therefore, needed.[51,54,55]

MIL-100(Cr) and MIL-47(V) have similar separation factors as Cu-btc, but lower working capacities. In the case of MIL-100(Cr), the lower working capacity results from the fact that the huge pore volume of the structure is not efficiently filled at 5 bar. On top of that, the regeneration of the CUS is difficult at 1 bar. NaX gives the best separation among the samples tested in our study, but has a low working capacity because its

  

isotherm is too steep. The highly polar character of NaX is beneficial for selectivity, but detrimental for regeneration.

Among the other MOFs selected from literature, UiO-66(Zr) and CAU-1(Al) (or $[Al_4(OH)_2(OMe)_4(bdc\text{-}NH_2)_3]$)[47] are best in the working capacity-vs.-separation factor ranking [The data on CAU-1 are unpublished in-house adsorption data. We acknowledge D. Farrusseng and M. Savonnet (IRCELyon) for providing the sample]. Both exhibit a 3D pore system with similar pore sizes (cages of $\approx$1 nm) and apertures (0.49 and 0.45 nm, respectively). These textural features lead to a good working capacity. The high separation factor of UIO-66[49] is surprising, as UiO-66 is supposedly nonpolar when dehydroxylated (no CUS accessible for $CO_2$ or CO, no polar functional groups). On the contrary, the separation factor of CAU-1, which is an amino-functionalized MOF, is relatively low. In a recent paper, Si et al.[56] found a higher adsorption capacity (probably because of better quality of the sample) and a $CO_2/CH_4$ selectivity of 28 at 273 K. The selectivity at 298 K is, however, significantly lower and agrees with our data. It remains puzzling why the amino substitution of the benzene ring of MOF ligands has a very positive effect on the $CO_2/CH_4$ selectivity in some structures, but not in others. For example, an amino-functionalized MIL-53(Al) has a very high $CO_2/CH_4$ selectivity, but recent work showed that the high selectivity is not a result of the strong affinity between $CO_2$ and the amino group, but rather arises from the fact that the amino group stabilizes the $CO_2$-phile NP form of MIL-53(Al).[57] For non-breathing MOFs, amino functionalization increased the $CO_2/CH_4$ selectivity of MIL-101,[58] improved significantly the $CO_2$ adsorption of MIL-125(Ti)[59] (or $[Ti_4(OH)_2(O)_4(bdc)_3]$, structure identical to CAU-1), but enhanced only slightly the capacity of UiO-66.[20] This subject certainly merits further investigation.

ZIF-8[60,61] (or $[Zn(MeIM)_2]$, MeIM = 2-methylimidazolate) is not sufficiently polar and, therefore, has a low capacity and a low separation factor. MIL-140(Zr)-A and $[Zn_2(ndc)_2(dpni)]$ (ndc = 1,4-naphthalenedicarboxylic acid; dpni = *N*,*N*′-di-(4-pyridyl)-1,4,5,8-naphthalene tetracarboxydiimide).[48] have the handicap of a low pore volume, which limits their adsorption capacity.

One can conclude that the most promising MOF adsorbents for biogas separation will probably be found within the group of MOFs with coordinatively unsaturated metal sites. They systematically outperform NaX in terms of working capacity and possibly also in terms of the separation factor for the CPO-27 family. Compared to activated carbons, MOFs systematically offer an improved capacity and a better quality of separation. Detailed PSA simulations and pilot tests will have to show whether the expected gain in performance with the above-mentioned CUS-MOFs is confirmed under real conditions. Further, an economic analysis needs to be conducted to judge whether the performance gain outweighs the potential drawbacks, such as the cost, difficulty of large scale synthesis, the long-term stability, etc.

### $CO_2$ capture in $H_2$ purification and in IGCC systems

The plot of separation factor vs. working capacity for $H_2$ purification with $CO_2$ capture looks similar to Figure 9 (it is shown in the Supporting Information). The main difference is that MIL-47(V) is now better ranked than MIL-100(Cr) because of the low $CO_2$/CO selectivity of the latter.

The situation for $CO_2$ capture in IGCC systems seems to be different, as we deal with a $CO_2$/CO separation at significantly higher pressures. For the "low pressure" case, that is, feed at 28 bar and desorption at 1 bar, the best separation factors are found for NaX and MIL-47(V). MIL-100(Cr) and Cu-btc exhibit lower $CO_2$/CO selectivities because of the relatively strong interaction of the CUS with CO. This result is qualitatively confirmed by breakthrough measurements. For high pressures, that is, feed at 57 bar, we could test the effect of desorption at $>$1 bar because the partial pressure of $CO_2$ in the feed is sufficiently high. Under these conditions (regeneration at 5 bar), the model calculations predict that MIL-100(Cr) should have the best performance among the 5 samples (Figure 10). Its large pore volume is well exploited at high partial pressure of $CO_2$ in the feed, and the shape of the isotherm (Figure 1) is favorable for desorption at $>$ 1 bar. Quite surprisingly, MIL-140(Zr)-A is predicted to have the highest separation factor for the IGCC case because of its very low affinity for CO.

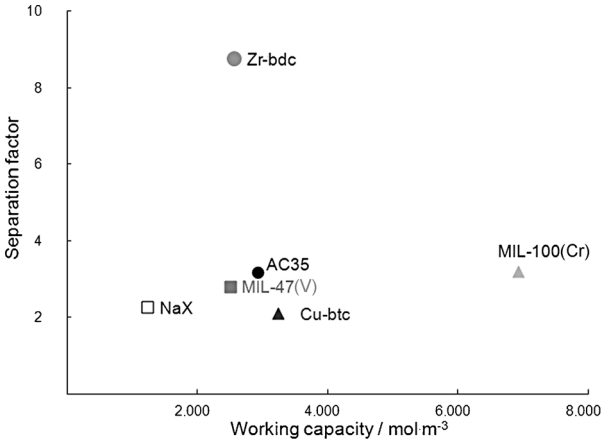


**Figure 10.** Separation factor vs. working capacity for $CO_2$ capture in IGCC systems. Adsorption pressure 57 bar, desorption pressure 5 bar.

### Estimation of adiabatic working capacity

PSA processes usually operate under adiabatic conditions. During the adsorption step, the heat released by exothermic adsorption increases the temperature of the bed, which reduces the adsorption capacity. Vice versa, the bed is cooled down during the desorption step because heat has to be provided to allow desorption. The decrease of temperature counteracts desorption. Both effects decrease the working capacity compared to the isothermal case. Therefore, the working capacities and separation factors should ideally be calculated

  

under adiabatic conditions. In this way, the best compromise between heat of adsorption, the adsorption capacity, and the selectivity can be defined. However, for calculating adiabatic adsorbate loadings, a temperature-dependent adsorption model is required, which is not trivial to obtain. It requires extensive temperature-dependent isotherm data, that is, an experimental effort that is not adapted for a screening phase.

As a first step towards accounting for heat effects, we have transformed the $CO_2$ isotherms into adiabates by using the enthalpy profiles of Figure 3 a. The heat released by adsorption was accounted for by calculating the temperature rise and the associated decrease of the adsorption capacity (see the Supporting Information for details). Figure 11 shows that the heat effects perturb the order of adsorption capacities considerably.

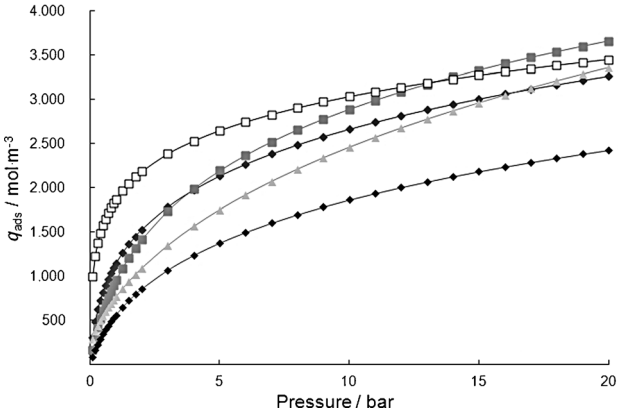


**Figure 11.** Adiabates of $CO_2$, calculated by starting from a temperature of 303 K. ◆ Cu-btc, ■: MIL-47(V), ▲: MIL-100(Cr), □: NaX, ◆: AC35.

The samples with the highest adsorption enthalpy, that is, MIL-100(Cr), Cu-btc, and NaX are strongly penalized, whereas MIL-47(V) rises in the ranking due to its low adsorption enthalpy.

We have further calculated the adiabatic working capacity of $CO_2$, between ($P_{ads}$; $T_0+\Delta T/2$) and ($P_{des}$; $T_0-\Delta T/2$); $P_{ads}=5$ bar, $P_{des}=1$ bar, and $T_0=303$ K (see Table 5). Surprisingly, the adiabatic working capacities of all evaluated samples are rather close. MIL-47(V) and MIL-100(Cr) are on top of the ranking because of the low adsorption enthalpy of the former and because of the high heat capacity of the latter. Unfortunately, it is for the moment not possible to verify these results experimentally because adiabatic operation would require considerably larger columns ($\approx 0.5$ m$^3$) and hence larger amounts of adsorbent, which we do not yet have at our disposal.

**Table 5.** Adiabatic working capacity of pure $CO_2$ between adsorption at 5 bar and $T_0+\Delta T/2$ and 1 bar and $T_0-\Delta T/2$; $T_0=303$ K.

| Adsorbent | $\Delta q_{CO_2}$ [mol m$^{-3}$] | $\Delta T$ [K] |
|---|---|---|
| MIL-47(V) | 1423 | 29.0 |
| Cu-btc | 1004 | 34.9 |
| MIL-100(Cr) | 1466 | 23.2 |
| AC35 | 981 | 32.7 |
| NaX | 787 | 22.7 |

### Flexible MOFs—the MIL-53 family

The flexible MOFs of the MIL-53 family have not been described here in our evaluation above because the breathing behavior asks for a special treatment. The detailed $CO_2/CH_4$ separation properties of the MIL-53 family have been described before,[62,63] but we want to sum up the essential conclusions here. MIL-53(Cr) is very $CO_2$ selective in its NP form, due to the strong interaction of $CO_2$ with hydroxyl groups in the inorganic chain, but the pore volume of the NP form is rather low, which limits the adsorption capacity. To exploit the potential adsorption capacity of MIL-53(Cr), the structure has to open to the LP form, which occurs at a partial pressure of $\approx 5$ bar $CO_2$. The LP form, however, loses its high selectivity for $CO_2$ and quite large amounts of $CH_4$ or CO can be coadsorbed after opening of the structure. We can suspect that, for any breathing MOFs with a large volume change between the NP and LP forms, gate opening by $CO_2$ will fatally allow other components to enter the pore structure. Hence, these materials will generally not be as selective as $CO_2$ adsorbents as could be expected from the single-component adsorption data. Moreover, breathing or gate opening, are systematically associated with an adsorption–desorption hysteresis, which is unfavorable for the regeneration of the adsorbent. We, therefore, think that MIL-53(Cr) is not the ideal adsorbent for $CO_2$ separations, as the origin of its selectivity is associated with a very specific adsorption geometry that is only possible in the NP form. The objective for future research must be to maintain a high $CO_2$ selectivity also in the LP form by increasing the affinity of the framework for $CO_2$. The very promising adsorption properties of MIL-47(V), which has nothing but an LP MIL-53 structure, indicate that this should not be an impossible task.

## Conclusions

The major challenge in finding improved adsorbents for $CO_2$ separations by means of PSA is to tune the $CO_2$ affinity. A high $CO_2$ affinity assures a high selectivity, but makes regeneration of the material difficult. NaX falls into this category. Low affinities are favorable for regeneration, but penalize selectivity and, at low pressures, also the capacity. This is the case of nonpolar adsorbents, such as activated carbons. We are, therefore, looking for adsorbents that are less polar than NaX, but more polar than activated carbons. The interesting conclusion of this study is that some MOF structures fall into this category, in particular MOFs with coordinatively unsaturated sites, such as Cu-btc, MIL-100, and based on literature data, also CPO-27. In particular, unsaturated Cu-sites offer an excellent compromise between $CO_2$ affinity and regenerability and thereby lead to best working capacities for medium pressure applications. A drawback of Cu-based carboxylate MOFs is, however, their moderate stability towards $H_2O$.

A second advantage of MOFs compared to NaX is that some of them have a higher porosity. It is fortuitous that Cu-btc and

  

MIL-100(Cr) fall into this category. Hence, they have a higher potential adsorption capacity per adsorbent volume. In the case of very large pore MOFs, such as MIL-100(Cr), the large pore volume may not be well exploited in applications where the partial pressure of $CO_2$ is fairly low. These large pore structures become very interesting, however, for high pressure applications, as for example in IGCC systems.

Coordinatively unsaturated sites are able to offer the medium $CO_2$ affinity that we are looking for, but our results indicate that the CUS also have relatively strong interactions with CO. This is a drawback for $CO_2$ separation in gas mixtures with high CO concentrations. For such applications, MOFs without accessible CUS, such as MIL-47(V) and UiO-66(Zr), may be more interesting. It is quite surprising that these two MOFs, which are supposedly less polar than the other MOFs considered, offer high adsorption capacities and good selectivities at medium to high pressures. MIL-47(V) itself is not viable for industrial applications because of its lack of stability, but UiO-66 was shown to have excellent thermal and hydrothermal stability.

On a laboratory scale, gas separations are usually carried out under isothermal conditions. Real PSA processes are adiabatic, and thermal effects are of utmost importance. They may turn the ranking of working capacities upside down (selectivities should be less affected). It is, therefore, dangerous to select adsorbents only based on measurements under isothermal conditions. Unfortunately, it is not at all trivial to realize adiabatic conditions in laboratory tests. Large amounts of adsorbent are needed for such tests, which is still a challenge for most MOF structures.

Finally, we would like to end by stating that the success of a MOF structure for $CO_2$ separations by means of PSA will not only depend on its technical performance, but also on the ease and cost of its preparation,[64] the availability of the starting materials, health and safety aspects (such as biodegradability and toxicity[65]), and on the long-term (chemical) stability of the material. The long-term stability of some otherwise very promising MOF structures, such as Cu-btc and MIL-47(V), may be a show-stopper for PSA applications, for which adsorbent lifetimes of five to ten years are generally expected.

## Acknowledgements

*The authors acknowledge the financial support of the French ANR "NOMAC" (ANR-06-CO2-008) and the European Union through the FP7 project 'MACADEMIA' (CP-IP-228862-2). The authors also thank the other partners of the "NOMAC" project (Drs. G. Maurin, F. Salles, A. Vimont, G. Clet, M. Daturi, and H. Jobic) for fruitful discussions. Jean-Pierre Courcy is acknowledged for carrying out part of the adsorption and breakthrough measurements, Catherine Lefebvre and Armelle Nigon (all IFPEN) for determining the heat capacities. Andrew Wiersum and Emily Bloch (LCP) are thanked for carrying out some of the calorimetry measurements.*

**Keywords:** adsorption · gas separation · metal-organic frameworks · structure–property relationship · zeolites

[1] J. D. Figueroa, T. Fout, S. Plasynski, H. McIlvried, R. D. Srivastava, *Int. J. Greenhouse Gas Control* **2008**, *2*, 9 – 20.
[2] S. Keskin, T. M. van Heest, D. S. Sholl, *ChemSusChem* **2010**, *3*, 879 – 891.
[3] C. W. Jones, E. J. Maginn, *ChemSusChem* **2010**, *3*, 863 – 864.
[4] D. M. D'Alessandro, B. Smit, J. R. Long, *Angew. Chem.* **2010**, *122*, 6194 – 6219; *Angew. Chem. Int. Ed.* **2010**, *49*, 6058 – 6082.
[5] A. Sayari, Y. Belmabkhout, R. Serna-Guerrero, *Chem. Eng. J.* **2011**, *171*, 760 – 774.
[6] G. Férey, C. Mellot-Draznieks, C. Serre, F. MILlange, J. Dutour, S. Surble, I. Margiolaki, *Science* **2005**, *309*, 2040 – 2042.
[7] M. Eddaoudi, J. Kim, N. Rosi, D. Vodak, J. Wachter, M. O'Keefe, O. M. Yaghi, *Science* **2002**, *295*, 469 – 472.
[8] C. Serre, F. MILlange, C. Thouvenot, M. Nogues, G. Marsolier, D. Louer, G. Férey, *J. Am. Chem. Soc.* **2002**, *124*, 13519 – 13526.
[9] K. Uemura, R. Matsuda, S. Kitagawa, *J. Solid State Chem.* **2005**, *178*, 2420 – 2429.
[10] T. Uemura, Y. Ono, Y. Hijikata, S. Kitagawa, *J. Am. Chem. Soc.* **2010**, *132*, 4917 – 4924.
[11] T. Devic, P. Horcajada, C. Serre, F. Salles, G. Maurin, B. Moulin, D. Heurtaux, G. Clet, A. Vimont, J. M. Greneche, B. Le Ouay, F. Moreau, E. Magnier, Y. Filinchuk, J. Marrot, J. C. Lavalley, M. Daturi, G. Férey, *J. Am. Chem. Soc.* **2010**, *132*, 1127 – 1136.
[12] Y. Zhao, H. Wu, T. J. Emge, Q. Gong, N. Nijem, Y. J. Chabal, L. Kong, D. C. Langreth, H. Liu, H. Zeng, J. Li, *Chem. Eur. J.* **2011**, *17*, 5101 – 5109.
[13] a) J. M. Simmons, H. Wu, W. Zhou, T. Yildirim, *Energy Environ. Sci.* **2011**, *4*, 2177 – 2185; b) K. Sumida, D. L. Rogow, J. A. Mason, T. M. McDonald, E. D. Bloch, Z. R. Herm, T.-H. Bae, J. R. Long, *Chem. Rev.* **2012**, *112*, 724 – 781.
[14] J. R. Li, Y. Ma, M. C. McCarthy, J. Sculley, J. Yu, H. K. Jeong, P. B. Balbuena, H. C. Zhou, *Coord. Chem. Rev.* **2011**, *255*, 1791 – 1823.
[15] G. D. Pirngruber, P. L. Llewellyn in *Metal Organic Frameworks: Applications from Catalysis to Gas Storage* (Ed.: D. Farrusseng), Wiley-VCH, Weinheim, **2011**, pp. 99 – 116.
[16] S. U. Rege, R. T. Yang, *Sep. Sci. Technol.* **2001**, *36*, 3355 – 3365.
[17] J. J. Low, A. I. Benin, P. Jakubczak, J. F. Abrahamian, S. A. Faheem, R. R. Willis, *J. Am. Chem. Soc.* **2009**, *131*, 15834 – 15842.
[18] K. A. Cychosz, A. J. Matzger, *Langmuir* **2010**, *26*, 17198 – 17202.
[19] L. Hamon, C. Serre, T. Devic, T. Loiseau, F. MILlange, G. Férey, G. De Weireld, *J. Am. Chem. Soc.* **2009**, *131*, 8775 – 8777.
[20] V. Guillerm, *PhD Thesis*, Université de Versailles, **2011**.
[21] K. Barthelet, J. Marrot, D. Riou, G. Férey, *Angew. Chem.* **2002**, *114*, 291 – 294; *Angew. Chem. Int. Ed.* **2002**, *41*, 281 – 284.
[22] S. S. Y. Chui, S. M. F. Lo, J. P. H. Charmant, A. G. Orpen, I. D. Williams, *Science* **1999**, *283*, 1148 – 1150.
[23] G. Férey, C. Serre, C. Mellot-Draznieks, F. MILlange, S. Surblé, J. Dutour, I. Margiolaki, *Angew. Chem.* **2004**, *116*, 6456 – 6461; *Angew. Chem. Int. Ed.* **2004**, *43*, 6296 – 6301.
[24] C. Serre, F. MILlange, S. Surble, G. Férey, *Angew. Chem.* **2004**, *116*, 6445 – 6449; *Angew. Chem. Int. Ed.* **2004**, *43*, 6285 – 6289.
[25] S. Bordiga, L. Regli, F. Bonino, E. Groppo, C. Lamberti, B. Xiao, P. S. Wheatley, R. E. Morris, A. Zecchina, *Phys. Chem. Chem. Phys.* **2007**, *9*, 2676 – 2685.
[26] L. Alaerts, M. Maes, P. A. Jacobs, J. F. M. Denayer, D. E. De Vos, *Phys. Chem. Chem. Phys.* **2008**, *10*, 2979 – 2985.
[27] P. L. Llewellyn, G. Maurin, *Comptes Rendus Chimie* **2005**, *8*, 283 – 302.
[28] J. A. Mason, K. Sumida, Z. R. Herm, R. Krishna, J. Long, *Energy Environ. Sci.* **2011**, *4*, 3030 – 3040.
[29] L. F. Song, C. H. Jiang, J. Zhang, L. X. Sun, F. Xu, W. S. You, Y. Zhao, Z. H. Zhang, M. H. Wang, Y. Sawada, Z. Cao, J. L. Zeng, *J. Therm. Anal. Calorim.* **2010**, *100*, 679 – 684.
[30] L. F. Song, C. H. Jiang, J. A. Zhang, L. X. Sun, F. Xu, Y. Q. Tian, W. S. You, Z. Cao, L. Zhang, D. W. Yang, *J. Therm. Anal. Calorim.* **2010**, *101*, 365 – 370.
[31] C. Serre, S. Bourrelly, A. Vimont, N. A. Ramsahye, G. Maurin, P. L. Llewellyn, M. Daturi, Y. Filinchuk, O. Leynaud, P. Barnes, G. Férey, *Adv. Mater.* **2007**, *19*, 2246 – 2251.

  

[32] A. Vimont, J. M. Goupil, J. C. Lavalley, M. Daturi, S. Surble, C. Serre, F. MILlange, G. Férey, N. Audebrand, *J. Am. Chem. Soc.* **2006**, *128*, 3218 – 3227.
[33] A. Vimont, A. Travert, P. Bazin, J. C. Lavalley, M. Daturi, C. Serre, G. Férey, S. Bourrelly, P. L. Llewellyn, *Chem. Commun.* **2007**, 3291 – 3293.
[34] G. Férey, C. Serre, T. Devic, G. Maurin, H. Jobic, P. L. Llewellyn, G. De Weireld, A. Vimont, M. Daturi, J. S. Chang, *Chem. Soc. Rev.* **2011**, *40*, 550 – 562.
[35] L. Grajciar, A. D. Wiersum, P. L. Llewellyn, J.-S. Chang, P. Nachtigall, *J. Phys. Chem. C* **2011**, *115*, 17925 – 17933.
[36] S. Bordiga, E. Garrone, C. Lamberti, A. Zecchina, C. O. Arean, V. B. Kazansky, L. M. Kustov, *J. Chem. Soc. Faraday Trans.* **1994**, *90*, 3367 – 3372.
[37] A. C. Kizzie, A. G. Wong-Foy, A. J. Matzger, *Langmuir* **2011**, *27*, 6368 – 6373.
[38] J. Liu, A. I. Benin, A. M. B. Furtado, P. Jakubczak, R. R. Willis, M. D. LeVan, *Langmuir* **2011**, *27*, 11451 – 11456.
[39] J. H. Cavka, S. Jakobsen, U. Olsbye, N. Guillou, C. Lamberti, S. Bordiga, K. P. Lillerud, *J. Am. Chem. Soc.* **2008**, *130*, 13850 – 13851.
[40] F. Salles, S. Bourrelly, H. Jobic, T. Devic, V. Guillerm, P. Llewellyn, C. Serre, G. Férey, G. Maurin, *J. Phys. Chem. C* **2011**, *115*, 10764 – 10776.
[41] F. Gul-E-Noor, B. Jee, A. Poppl, M. Hartmann, D. Himsl, M. Bertmer, *Phys. Chem. Chem. Phys.* **2011**, *13*, 7783 – 7788.
[42] J. Liu, Y. Wang, A. I. Benin, P. Jakubczak, R. R. Willis, M. D. LeVan, *Langmuir* **2010**, *26*, 14301 – 14307.
[43] L. Hamon, E. Jolimaitre, G. D. Pirngruber, *Ind. Eng. Chem. Res.* **2010**, *49*, 7497 – 7503.
[44] L. J. Murray, M. Dinca, J. R. Long, *Chem. Soc. Rev.* **2009**, *38*, 1294 – 1314.
[45] Y. H. Hu, L. Zhang, *Adv. Mater.* **2010**, *22*, E117 – E130.
[46] S. Tedds, A. Walton, D. P. Broom, D. Book, *Faraday Discuss.* **2011**, *151*, 75 – 94.
[47] T. Ahnfeldt, N. Guillou, D. Gunzelmann, I. Margiolaki, T. Loiseau, G. Férey, J. Senker, N. Stock, *Angew. Chem.* **2009**, *121*, 5265 – 5268; *Angew. Chem. Int. Ed.* **2009**, *48*, 5163 – 5166.
[48] Y. S. Bae, K. L. Mulfort, H. Frost, P. Ryan, S. Punnathanam, L. J. Broadbelt, J. T. Hupp, R. Q. Snurr, *Langmuir* **2008**, *24*, 8592 – 8598.
[49] Q. Y. Yang, A. D. Wiersum, H. Jobic, V. Guillerm, C. Serre, P. L. Llewellyn, G. Maurin, *J. Phys. Chem. C* **2011**, *115*, 13768 – 13774.
[50] J. Pérez-Pellitero, H. Amrouche, F. R. Siperstein, G. Pirngruber, C. Nieto-Draghi, G. Chaplais, A. Simon-Masseron, D. Bazer-Bachi, D. Peralta, N. Bats, *Chem. Eur. J.* **2010**, *16*, 1560 – 1571.
[51] P. D. C. Dietzel, V. Besikiotis, R. Blom, *J. Mater. Chem.* **2009**, *19*, 7362 – 7370.
[52] H. Wu, J. M. Simmons, Y. Liu, C. M. Brown, X. S. Wang, S. Ma, V. K. Peterson, P. D. Southon, C. J. Kepert, H. C. Zhou, T. Yildirim, W. Zhou, *Chem. Eur. J.* **2010**, *16*, 5205 – 5214.
[53] P. D. C. Dietzel, Y. Morita, R. Blom, H. Fjellvag, *Angew. Chem.* **2005**, *117*, 6512 – 6516; *Angew. Chem. Int. Ed.* **2005**, *44*, 6354 – 6358.
[54] D. Britt, H. Furukawa, B. Wang, T. G. Glover, O. M. Yaghi, *Proc. Natl. Acad. Sci. USA* **2009**, *106*, 20637 – 20640.
[55] R. Krishna, J. R. Long, *J. Phys. Chem. C* **2011**, *115*, 12941 – 12950.
[56] X. Si, C. Jiao, F. Li, J. Zhang, S. Wang, S. Liu, Z. Li, L. Sun, F. Xu, Z. Gabelica, C. Schick, *Energy Environ. Sci.* **2011**, *4*, 4522 – 4527.
[57] E. Stavitski, E. A. Pidko, S. Couck, T. Remy, E. J. M. Hensen, B. M. Weckhuysen, J. Denayer, J. Gascon, F. Kapteijn, *Langmuir* **2011**, *27*, 3970 – 3976.
[58] P. Serra-Crespo, E. V. Ramos-Fernandez, J. Gascon, F. Kapteijn, *Chem. Mater.* **2011**, *23*, 2565 – 2572.
[59] M. Dan-Hardi, C. Serre, T. Frot, L. Rozes, G. Maurin, C. Sanchez, G. Férey, *J. Am. Chem. Soc.* **2009**, *131*, 10857 – 10859.
[60] K. S. Park, Z. Ni, A. P. Cote, J. Y. Choi, R. D. Huang, F. J. Uribe-Romo, H. K. Chae, M. O'Keeffe, O. M. Yaghi, *Proc. Natl. Acad. Sci. USA* **2006**, *103*, 10186 – 10191.
[61] X. C. Huang, Y. Y. Lin, J. P. Zhang, X. M. Chen, *Angew. Chem.* **2006**, *118*, 1587 – 1589; *Angew. Chem. Int. Ed.* **2006**, *45*, 1557 – 1559.
[62] L. Hamon, P. L. Llewellyn, T. Devic, A. Ghoufi, G. Clet, V. Guillerm, G. D. Pirngruber, G. Maurin, C. Serre, G. Driver, W. Van Beek, E. Jolimaitre, A. Vimont, M. Daturi, G. Férey, *J. Am. Chem. Soc.* **2009**, *131*, 17490 – 17499.
[63] V. Finsy, L. Ma, L. Alaerts, D. E. De Vos, G. V. Baron, J. F. M. Denayer, *Microporous Mesoporous Mater.* **2009**, *120*, 221 – 227.
[64] A. Czaja, E. Leung, N. Trukhan, U. Müller in *Metal-Organic Frameworks: Application from Catalysis to Gas Storage* (Ed.: D. Farrusseng), Wiley-VCH, Weinheim, **2011**, pp. 339 – 352.
[65] P. Horcajada, T. Chalati, C. Serre, B. Gillet, C. Sebrie, T. Baati, J. F. Eubank, D. Heurtaux, P. Clayette, C. Kreuz, J. S. Chang, Y. K. Hwang, V. Marsaud, P. N. Bories, L. Cynober, S. Gil, G. Férey, P. Couvreur, R. Gref, *Nat. Mater.* **2010**, *9*, 172 – 178.

Received: November 9, 2011
Published online on March 21, 2012

  